

A study of SnS thin films and its suitability for photovoltaic application based on the existence of persistent photocurrent

Yashika Gupta^{a,b}, P.Arun^{a,1,*}

^aMaterial Science Research Lab., S.G.T.B. Khalsa College,
University of Delhi, Delhi 110007, INDIA

^bDepartment of Electronic Science, University of Delhi-South Campus,
New Delhi 110021, INDIA

arXiv:1502.05335v1 [cond-mat.mtrl-sci] 18 Feb 2015

Abstract

Tin Sulphide is a layered compound which retains its structure when deposited as thin films by thermal evaporation. The films were found to have oriented growth with the direction of orientation changing with film thickness. The film's morphology was found to change with orientation. The poor conductivity of the thicker samples made it difficult to make photocunductivity characterisation. However, unlike reported the thinner samples showed photo-sensitivity to be independent of film thickness and grain size with a high presistent photocurrent. With their absorption, photosensitivty, optimum band-gap and traps within the band-gap giving the charge carriers a longer life-time, thin samples of tin sulphide gives adequate scope designing efficient photovoltaics. The refractive index was modeled using Sellmeir's model, while most of the previous studies talk of Wemple-DiDomenico single oscillator model or Cauchy's dispersion relation. The Sellmeir's fitting parameters are reported which can be of use in ellipsometric studies.

Keywords:

1. Introduction

Search for an abundant, inorganic and non-toxic material with good absorption coefficient at relatively low thicknesses in solar cell applications has narrowed down to Tin Sulphide (SnS) [1, 2]. SnS has been successfully fabricated by chemical methods [3]-[6], spray pyrolysis [7]-[9], sputtering [10], thermal evaporation [2],[11]- [13] and electron beam assisted evaporation [14]. The band-gap of the films were reported to lay between 1.3-2.5 eV [1],[15]-[18] depending on the fabrication technique. With band-gap laying in this range, SnS is capable of utilizing the visiable range of solar radiation falling on the earth's surface.

Literature shows that the present efforts are directed towards finding an appropriate second layer

for the diode formation with SnS. The best efficiency reported is 4.4% with Zinc Oxysulphide, Zn(O,S), acting as the n-layer [19]. Annealing [20] and/or sulphurization [21] of the SnS layer has also been suggested to improve the SnS solar cell's efficiency. However, directed fundamental characterization of SnS films especially on presistant photoconductivity is absent. In fact a search of the literature only shows a couple of articles on SnS presistant photoconductivity [22, 23]. Considering a long carrier lifetime (in relation to photoconductivity) would assist in improving the photovoltaics preformance [24], an in-depth correlation of carrier lifetime with film parameters is a must. We have tried to address this in the present work.

The present work reports the fabrication of p-type SnS thin films via thermal evaporation method on glass substrate maintained at room temperature. Characterization of the films shows that the properties, both electrical and optical, are strongly related

*Corresponding author

Email address: arunp92@physics.du.ac.in (P.Arun)

¹(T) +91 11 29258401 (F) +91 11 27666220

to the orientation of the unit cell which in turn depends on the film thickness.

2. Experimental

Thin SnS films of varying thicknesses were grown at rates greater than 2 nm/sec on microscopy glass substrate maintained at room temperature by thermal evaporation of SnS pellets at vacuums better than $\approx 4 \times 10^{-5}$ Torr using a Hind High Vac (12A4D) coating unit. The starting material was SnS powder of 99.99% purity provided by Himedia (Mumbai). The thicknesses of the films were measured using Dektak surface profiler (150). Bruker D8 X-ray Diffractometer with copper target ($\text{CuK}\alpha$ radiation, $\lambda \sim 1.5406 \text{ \AA}$) and Transmission Electron Microscopy (Technai T30U Twin) was used to determine the structure/crystallinity of the samples. The surface morphology of the samples was compared using a Field Emission-Scanning Electron Microscope (FE-SEM FEI-Quanta 200F) at an accelerating voltage of 10 kV. The optical studies of the films were recorded using an UV-Vis Double Beam Spectrophotometer (Systronics 2202). Hot-spot probe method was used to determine the conductivity type of the films, which without exception showed that the as-grown films were p-type in nature.

The photoconductivity experiments were carried out at room temperature using a source meter SMU-01 of Marine (India). A tungsten lamp was used as our light source. Contacts were made using silver paste which is known to give good ohmic contacts with SnS [25, 26]

3. Results and Discussion

3.1. The Structural and Morphological Analysis

Fig 1 shows the X-Ray diffractograms of various samples whose thickness lie between 450 to 1680 nm. All the peak positions matched with those listed in ASTM Card No 79-2193 for SnS, having orthorhombic structure with lattice constants $a \approx 5.673$, $b \approx 5.75$ and $c \approx 11.76 \text{ \AA}$. As can be seen from the X-Ray diffractograms there is a change in orientation with increasing film thickness. Texture coefficient was estimated to determine the preferred

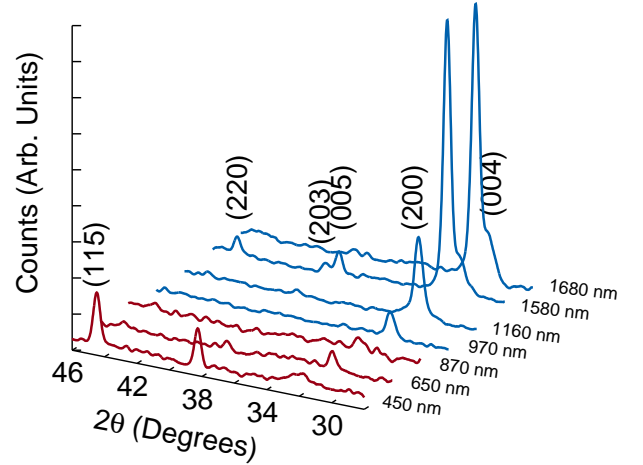


Figure 1: X-ray diffraction pattern

orientation of crystallites in the as-deposited films using the formula

$$T_{hkl} = \frac{\left[\frac{I_{hkl}}{I_{o(hkl)}} \right]}{\frac{1}{N} \sum_i \left[\frac{I_{hkl}}{I_{o(hkl)}} \right]_i}$$

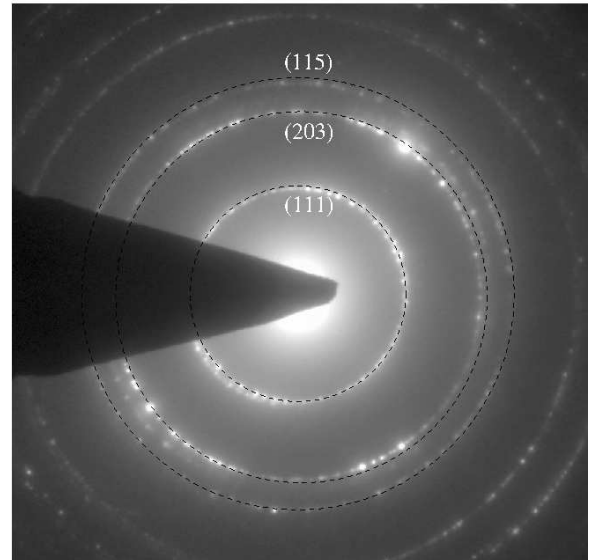


Figure 2: SAED micrograph confirms the sample's crystallinity. Major rings are marked and Miller indices indicated.

where T_{hkl} is the texture coefficient of (hkl) plane. This is evaluated using the intensity of the (hkl)

plane (I_{hkl}) obtained experimentally from the X-ray diffractograms while $I_{o(hkl)}$ is the intensity listed in the ASTM Card for the corresponding (hkl) peak and ‘N’ is the total number of diffraction peaks obtained in X-Ray diffraction. Preferential orientation (hkl) plane would have large texture coefficient compared to the other planes. We obtained $T_{005} \approx 2.5$ and $T_{200} \approx 3.35$ for 450 nm and 1680 nm films respectively, showing a shift from (005) orientation to (200) as film thickness increases. The Miller indices suggests that the film’s orientation moves from ‘xy’ layers parallel to the substrate (i.e. ‘c’ or the long axis perpendicular to the substrate) to an orientation where the ‘xy’ layers are perpendicular to the substrate (long/ ‘c’ axis parallel to the substrate).

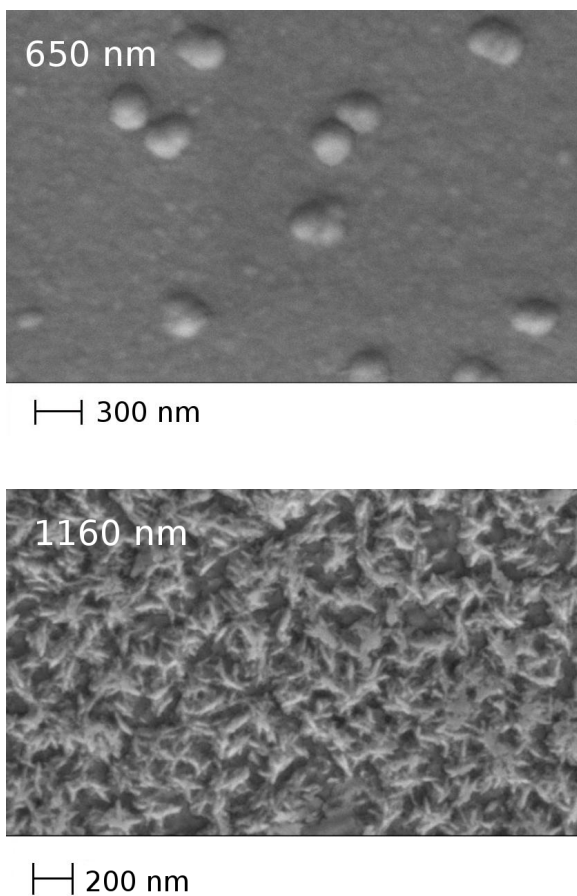


Figure 3: SEM micrograph.

To confirm the crystalline nature of the grown films, we did a Selected Area Electron Diffraction (SAED) analysis of our 650 nm sample using a Transmission Electron Microscope (Fig 2). The sharp rings confirm the crystallinity of our sam-

ples. The inner most ring corresponds to (111) plane, while the second and third ring correspond to the (203) and (115) peaks of our X-ray diffractograms (Fig 1), the (111) peak did not show in XRD. The SEM micrographs show two different morphologies, where thinner films showed spherical grains and thicker films exhibited ‘needle’ shaped morphology (fig 3). The needle shaped morphology [27]-[30] is typical when the ‘c’ or long axis is parallel to the substrate, thus confirming our assertion made while interpreting our X-Ray diffraction results.

The grain size of the SnS samples were determined from the XRD peaks according to the Scherrers formula [31]

$$D = \frac{0.9\lambda}{FWHM\cos\theta}$$

where ‘D’ is the grain size, λ is the wavelength of the X-ray used ($\lambda = 1.5406\text{\AA}$), FWHM is Full Width at Half Maximum intensity of the diffraction peaks and θ is the Bragg’s angle. Fig 4 shows the variation of grain size with film thickness. Initially, the grain

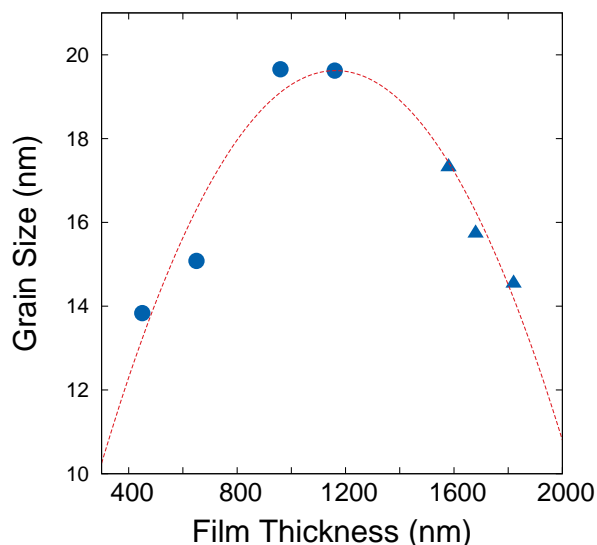


Figure 4: Variation of grain size with thickness. Circles indicate grains with spherical morphology and triangles indicate needle-shaped grains.

size increases with the thickness however, on reaching a maximum value it shows a decreasing trend with the film thickness. Co-relating with our SEM micrographs, we find that it is at this ‘‘point of inversion’’ thickness that the grain morphology changes from spherical to needle-shaped.

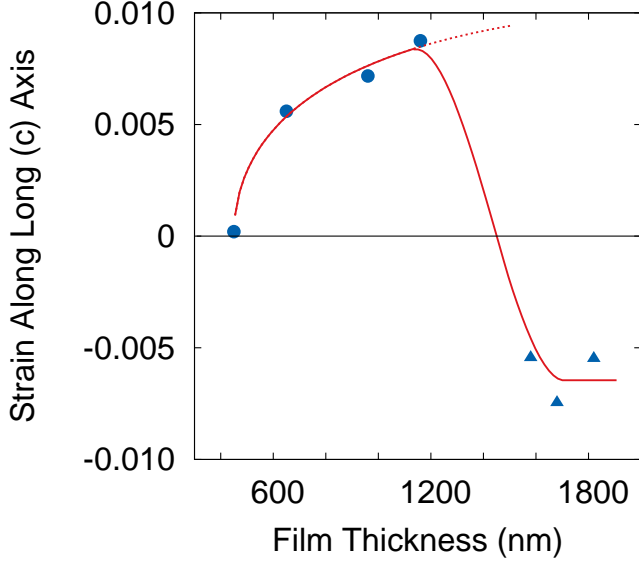


Figure 5: Variation of stress along the long ('c') axis with the film thickness. Circles indicate grains with spherical morphology and triangles indicate needle-shaped grains. Lines are only visual aids to show trend in variation.

To study this variation in grain size with changing morphology, lattice parameters were calculated using the following formulae [31]

$$\frac{1}{d^2} = \frac{h^2}{a^2} + \frac{k^2}{b^2} + \frac{l^2}{c^2} \quad (1)$$

where a, b, c are the lattice parameters and (hkl) are the Miller indices reported in the ASTM card. It was observed that a residual stress acts along the 'c-axis' of the orthorhombic SnS unit cell while the lattice parameters 'a' and 'b' were same as reported in the ASTM Card indicating no stress along these directions. The strain along the 'c' direction can be estimated using

$$\delta = \frac{c_{exp} - c_{ASTM}}{c_{ASTM}} \quad (2)$$

where 'c_{exp}' is the experimentally obtained long lattice parameter and 'c_{ASTM}' is that of a single crystal.

The study of strain with film thickness shows an interesting trend (fig 5). Films with spherical grains show tensile strain (or tensile residual stress) which increases with film thickness. Infact it shows a near parabolic trend with film thickness, with rate

of change shallowing as thickness increases (lines in fig 5 are for visual aid). This may explain the increase in grain size with film thickness. However, the films with the needle-shaped grains show compressive stress acting on it. The magnitude of residual stress seem to be constant with film thickness. The variation in residual stress with film thickness would indicate that the nature of residual stress changes with the long ('c') axis changing its orientation from perpendicular to the substrate (tensile stress) to parallel to the substrate (compressive stress). This curve suggests that the change in orientation takes place in films of thicknesses greater than 1160 nm.

3.2. Photoconductivity

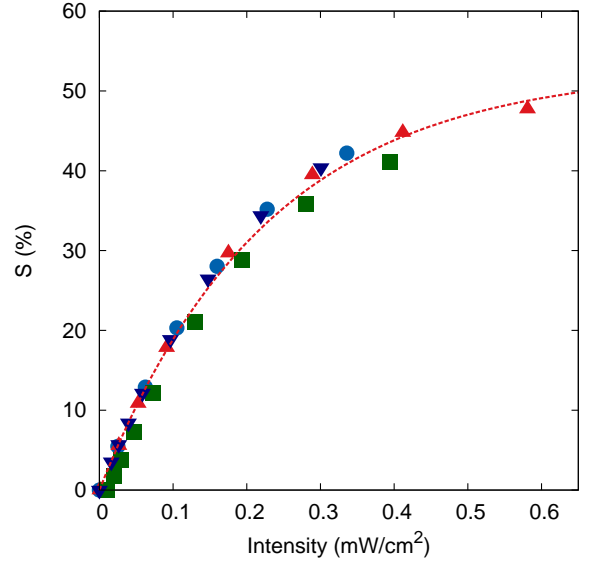


Figure 6: Plot shows variation of $(\alpha h\nu)^2$ with $h\nu$ for two different film thicknesses (450 and 1820 nm). Extrapolating the best fit line to the X-axis at $y=0$ gives the band gap of the respective films.

To study the photoconductivity of the films, the I-V characteristics of the sample's measured with them exposed under a tungsten bulb. Interestingly, the resistivity of the thicker films ($d \geq 1160$ nm) were found to be very high (beyond the measuring capability of the instrument). Similiar observation was made by Wang et al [32]. Considering that there is a sudden change in resistivity as the film thickness is increased beyond 1160 nm, we believe this exceptionally high resistivity is related to the grain orientation (as seen in our structural analysis, thicker samples have 'xy' plane perpendicular to the substrate).

Sinsermsuksakul et al [33] have shown that the mobility of charge carriers is significantly lower along the direction of Van der Waals forces. Hence, with electrodes made on the film's surface, we can appreciate the high resistance in thick SnS samples.

“Sensitivity” (S) is usually used as a figure of merit while discussing the photoconductivity of films and is given as [34]-[37]

$$S = \left(\frac{\sigma_L - \sigma_D}{\sigma_D} \right) \quad (3)$$

σ_L and σ_D is the films conductivity measured when exposed to light (L) and in dark (D) respectively. Sensitivity, hence is a measure of how much conduction increases in a sample with light intensity. The increase in conductivity maybe due to an increase in charge carriers [38, 39] or due to change in mobility [40]. From the charge carriers generated on illumination, a part would recombine with the respective opposite charges, thereby reducing the barrier potential at grain boundaries. This inturn would lead to an increase in the charge carrier's mobility. This is called grain boundary modulation [36]. The photoconductivity is given as [37]

$$\Delta\sigma = q(\Delta p)\mu + qp(\Delta\mu)$$

where ‘p’ is the charge carrier concentration (here restricted to holes considering p-type material is under discussion) and ‘q’ charge associated with single charge carrier, while μ is the carrier's mobility. Fig 6 shows the variation of sensitivity with intensity for four different thicknesses (less than 1160 nm) of polycrystalline samples whose grain size were different. As can be noticed, all the experimental data irrespective of the grain size follows the same trend. This would suggest that the sensitivity of p-SnS is independent of grain size, thus ruling out barrier modulation [40]. Thus, any increase in conductivity is due to increase in photo-conductors or carriers created by illumination. The above equation reduces to

$$\Delta\sigma = q(\Delta p)\mu$$

Fig 6 is also indicative of the fact that sensitivity is dependent on the illumination intensity. In fact it

is functionally given as [41, 22]

$$S \propto I^\gamma \quad (4)$$

where ‘I’ represents the illumination intensity. The exponential factor γ can be evaluated from the slope of the straight line obtained when fig 6 is plot on a logarithmic scale. For our data we obtain $\gamma = 0.876$, where $\gamma < 1$ indicates existence of traps within the bandgap and also the presence of bimolecular recombination (recombination on band-gap transition) [36, 42].

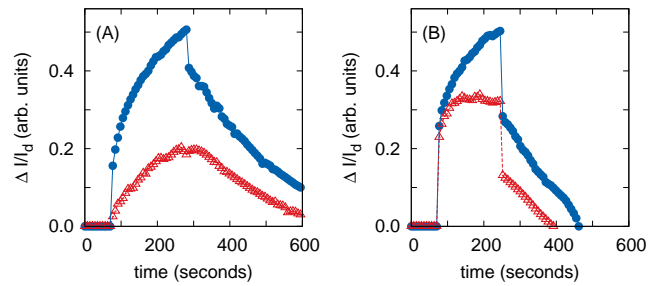


Figure 7: Variation of photocurrent with time for films of various thicknesses.

The existence of traps can also be appreciated from the rise and decay of photo-current. Photo-current Decay (PCD) measurements of our samples were made by applying a constant bias of 10V across them. Before illumination, the samples were maintained in dark for ≈ 70 s. The photo-current was measured during illumination for $t > 150$ s, followed by which we observed the current decay under the dark. Measurements were made till the original dark current was achieved. Unlike sensitivity, two trends were obtained, for (a) thinner samples ($d \leq 650$ nm) and (b) thicker samples ($d \geq 870$ nm).

The vertical rise and drop in current upon switching illumination ON and OFF respectively is a result of charge carriers crossing the band-gap with no contribution of traps. Whereas, the exponential rise and decay is trap assisted photo-current. The trap assisted photo-current or the persistent photo-conductivity (PPC) is dominant in thinner samples as compared to the thicker samples, as is evident by the larger vertical change regions of the curve. The persistent current is given by the equation [43, 44] as

$$I(t) = I_d + A_o \exp \left[\left(-\frac{t}{\tau} \right)^\beta \right] \quad (5)$$

Table I: Decay time constants of various films obtained by curve fitting eqn (5) to photo-current data.

Thickness (nm)	τ (seconds)
450	234.65
650	207.47
870	133.24
970	90.30

where I_d is the initial dark current, τ the decay-time constant and ' β ' represents the stretching exponent constant ($0 < \beta < 1$). The τ values obtained by curve fitting are listed in Table I. The large decay time indicates existence of trap centers within the forbidden band-gap of the film [23]. These trap centers increases the carrier life-time [45] in the as-grown p-SnS thin films. We find the charge carrier life-time systematically decreases as film thickness increases. Considering an increased life-time implies a reduced recombination rate allowing more time for the carriers to move without recombination, the material with long carrier life-time and good sensitivity would be a useful material for photovoltaics [24].

3.3. Optical Properties

3.3.1. Refractive Indices

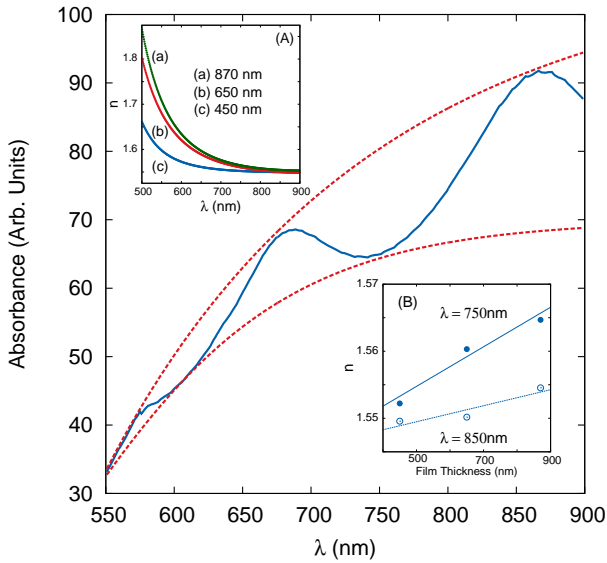


Figure 8: Plot shows variation of $(\alpha h\nu)^2$ with $h\nu$ for two different film thicknesses (450 and 1820 nm). Extrapolating the best fit line to the X-axis at $y=0$ gives the band gap of the respective films.

The refractive indices of the films were evaluated for different wavelengths using the standard Swanepoel's method [46, 47] from the transmission spectra of the samples. Swanepoel's method involves drawing envelopes connecting the extrema points of the the interference fringes appearing in the transmission spectra (see fig 8). Interestingly, these fringes did not appear in samples whose thickness was more than 1160 nm. Again, like our observation made on photoconductivity, films with thicknesses above 1160 nm coinciding with structural orientation change, shows a marked change in behavior. In this study, due to lack of fringes in thicker samples and limitations imposed by the technique, we report the variation of refractive indices seen in just three of our samples.

The inset (A) of fig 8 shows the variation of refractive indices of the three samples with wavelength. The dispersive trend of the three films look similiar. In fact the trend follows the Sellmeir relation [48] (curve fits have co-relation of 0.998) given below:

$$n^2 = A + \sum_j \frac{B_j \lambda^2}{\lambda^2 - C_{oj}} \quad (6)$$

Sellmeir model pictures the solid to be made of dipole oscillators with 'j' natural oscillation frequencies, given by $\omega_{oj} = 2\pi c/\lambda_{oj}$ (in above equation $\omega_{oj} = 2\pi c/\sqrt{C_{oj}}$). Interestingly, our results suggest SnS film's consist of single oscillators, all oscillating at frequencies corresponding to energies within 2.72-2.83 eV. This is well above the sample's known band-gap (which we shall discuss below), however the Sellmeir "oscillators" do not absorb away from the natural frequencies (our data is restrict for $\lambda \geq 500$ nm) and have zero broadening of the Lorentz absorption peak. This implies that the refractive index is a real number with $\epsilon_2 = 0$. Table II gives the coefficients of eqn 6 that fit to the experimental results which can be used for model fitting during ellipsometric studies. An increasing 'B' with film thickness suggests that the refractive index of the samples increases with film thickness for all wavelengths (see inset B of fig 8).

While our data clear shows that the refractive index fits Sellmeir's model, previous works have reported SnS follows Cauchy's dispersion relation [49]

Table II: Comparison of properties of SnS based solar cells from the literature listed in order of increasing efficiency.

Film Thickness (nm)	A	B ₁	C ₀₁ (×10 ⁵) nm ²
450	2.278	0.0834	2.08
650	1.983	0.3006	1.92
870	1.963	0.3180	1.99

and Wemple-DiDomenico single oscillator model for refractive index [50].

3.3.2. Band-gap Variation

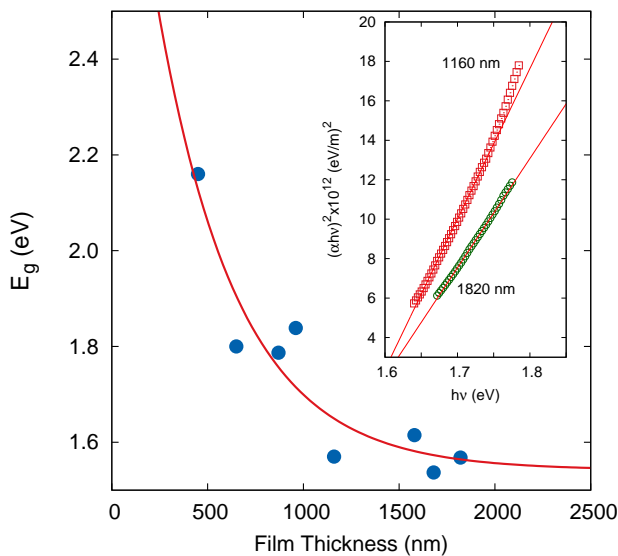


Figure 9: Plot shows variation of $(\alpha hv)^2$ with hv for two different film thicknesses (450 and 1820 nm). Extrapolating the best fit line to the X-axis at $y=0$ gives the band gap of the respective films.

The absorption spectra of the as-grown SnS films were studied in the wavelength range 300-900 nm. The band gaps of the films were evaluated from the absorption spectrum using the standard Tauc method [51]. Although SnS is reported to have both direct and indirect band-gaps [52], we obtained straight line fits only for plots between $(\alpha hv)^2$ and hv (see inset of fig 9), where ' α ' is the absorption coefficient and hv . This suggests that our p-SnS as-grown films have allowed direct band-gap [53]. The band-gap shows an exponential decrease with film thickness attaining the value of bulk samples (≈ 1.54 eV [54]-[56]) for thicknesses greater than 1500 nm.

4. Conclusions

Tin Sulphide (SnS) thin films were fabricated by thermal evaporation on glass substrates maintained at room temperature. The films were found to be nano-crystalline with layered structure, whose layers were found to be either parallel to the substrate or perpendicular to it depending on the film thickness. The orientation was found to have an effect on the film's morphology and its properties, such as electrical conductivity. The poor conductivity of thicker films caused by layers being perpendicular to the substrate made it impossible to study the photoconductivity of these samples. However, thinner samples showed good photo-sensitivity and we observed persistent photoconductivity in them. This indicates the existence of traps within the forbidden energy gap of thin samples. The charge carrier's life time was found to decrease with increasing film thickness. This would imply an improved photovoltaic performance in very thin samples of SnS with charge carriers reaching their respective electrodes without recombination. The optical studies showed a 2.2 eV band-gap for the thinner SnS films with large refractive index following Sellmeier's dispersion relation, ideally suited for simple photovoltaics and plasmonic photovoltaics using SnS as the absorbing layer.

Acknowledgement

One of the authors (YG) would like to express her gratitude to DST (India) for the financial assistance in terms of fellowship under the INSPIRE program (Fellowship No. IF131164).

References

- [1] C. Gao, H. Shen, Z. Shen, Mater. Lett **65**, (2011) 1143.
- [2] H. Noguchi, A. Setiyadi, H. Tanamura, T. Nagatomo and O. Omoto, Sol. Energy Mater. Sol. Cells **35**, (1994) 325.
- [3] Y. Wang, H. Gong, B. Fan and G. Hu, J. Phys. Chem. C **114**, (2010) 3256.
- [4] Y. Wang, Y.B.K. Reddy and H. Gong, J. Electrochem. Soc. **156**, (2009) H157.
- [5] D. Avellaneda, G. Delgado, M.T.S. Nair and P.K. Nair, J. Electrochem. Soc. **155**, (2008) D517.
- [6] M.T.S. Nair and P.K. Nair, Semicond. Sci. Tech. **6**, (1991) 132.
- [7] K.N. Reddy and K.T.R. Reddy, Mater. Chem. Phys. **102**, (2007) 13.

- [8] K.T.R.Reddy, K.N.Reddy and R.W.Miles, *Sol. Energy Mater. Sol. Cells* **90**, (2006) 3041.
- [9] E. Guneri, C. Gumus, F. Mansur, F. Kirmizigul, *J. Optoelectron. Adv. Mat.* **3**, (2009) 383.
- [10] S.Kamoshida, S.Suzuki, S., Japan Patent JP 08176814, A2, 1996.
- [11] M.M.El-Nahass, H.M.Zeyada, M.S.Aziz and N.A.El-Ghamaz, *Opt. Mater.* **20**, (2002) 159.
- [12] M.Devika, N.K.Reddy, S.Reddy, Q.Ahsanulhaq, K.Ramesh, E.S.R.Gopal, K.R.Gunasekhar and Y.B.J.Hahn, *J. Electrochem. Soc.* **155**, (2008) H130.
- [13] O.E. Ogah, G. Zoppi, I. Forbes, R.W. Miles, *Thin Solid Films* **517**, (2009) 2485.
- [14] A.Tanusevski and D.Poelman, *Sol. Energy Mater. Sol. Cells* **80**, (2003) 297.
- [15] M.R. Fadavieslam, N. Shahtahmasebi, M. Razaee-Roknabadi, M.M. Bagheri-Mohagheghi, *Phys. Scripta* **84**, (2011) 035705.
- [16] S. Sohila, M. Rajalakshmi, C. Ghosh, A.K. Arora, C. Muthamizhchelvan, *J. Alloy Compd.* **509**, (2011) 5843.
- [17] S.Cheng, G. Conibeer, *Thin Solid Films* **520**, (2011) 837.
- [18] A. Gomez, H. Martinez, M. Calixto-Rodriguez, D. Avalenda, P.G. Reyes, O. Flores, *J Mater. Sci. Eng. B* **3**, (2013) 352.
- [19] P. Sinsersuksakul, L. Sun, S.W. Lee, H.H. Park, S.B. Kim, C. Yang, R.G. Gordon, *Adv. Energy Mater.* (2014), doi:10.1002/aenm.201400496.
- [20] H. Li, S. Cheng, J. Zhang, W. Huang, H. Zhai, H. Jia, *WJCMF*, **5** (2015) 10.
- [21] M.V. Reddy, G. Sreedevi, C. Park, R.W.Miles, K.T. Reddy, *Curr. Appl. Phys.* (2015), doi:10.1016/j.cap.2015.01.022.
- [22] J.B. Johnson, H. Johnes, B.S. Latham, J.D. Parker, R.D. Engelken, C. Barber, *Semicond. Sci. Tech.* **14**, (1999) 501.
- [23] F. Jiang, H. Shen, J. Jiao, *ECS JSS* **2**, (2013) 478.
- [24] C. Soci, D. Moses, Q.H. Xu and A.J. Heeger, *Phys. Rev. B* **72**, (2005) 245204.
- [25] P. Pramanik, P.K. Basu, S. Biswas, *Thin Solid Films* **150**, (1987) 269.
- [26] N. Sato, M Ichimura, E. Arai, Y. Yamazaki, *Sol. Energy Mater. Sol. Cells* **85**, (2005) 153.
- [27] E. Guneri, F. Gode, C. Ulutas, F. Kirmizigul, G. Altindemie, C. Gumus, *Chalcogenide Lett.* **7**, (2010) 685.
- [28] C. Gao, H. Shem, L. Sun, *Appl. Surf. Sci.* **257**, (2011) 6750.
- [29] T. Sajeesh, A. Sherian, C. Kartha, K. Vijayakumar, *Energy Procedia* **15**, (2012) 325.
- [30] J. Park, M. Song, W.M. Jung, W.Y. Lee, J. Lee, H. Kim, I. Wunshim, *Bull. Korean Chem. Soc.* **33**, (2012) 3383.
- [31] B.D. Cullity, S.R. Stock, "Elementary of X-Ray Diffraction", 3rd Ed., Prentice-Hall Inc (NJ, 2001).
- [32] Y. Wang, Y.B.K. Reddy and H. Gong, *J. Electrochem. Soc.* **156**, (2009) H157.
- [33] P. Sinsersuksakul, J. Heo, W. Noh, A.S. Hock and R.G. Gordon, *Adv. Energy Mater.* **102** (2011) 1116.
- [34] R.H. Bube, "Photoelectronic properties of Semiconductors", Cambridge University Press (UK 1992).
- [35] Q. Feng, X Jinzhong, K. Jincheng, Y Lianjie, K. Lingde, W. Guanghua, L. Xiongjun, Y. Lili, L. Cong, J. Rongbin, *J Semicond.* **32**, (2011) 3.
- [36] P.K. Kalita, *Pramana-J. Phys.* **60**, (2003) 1242.
- [37] N.B. Kotadiya, A.J. Kothari, D. Tiwari, T.K. Chaudhuri, *Appl. Phys. A.* **108**, (2012) 819.
- [38] R.L. Petritz, *Phys. Rev.* **104**, (1956) 1508.
- [39] J.F. Woods, *Phys. Rev.* **106**, (1957) 235.
- [40] J.C. Slate, *Phys. Rev.* **103**, (1956) 1631.
- [41] J.J. Schellenberg, K.C. Kao, *J. Phys. D: Appl. Phys.* **21**, (1988) 1764.
- [42] Neetu, M. Zulfequar, *Indian J Pure and Appl. Phys.* **52**, (2014) 53.
- [43] X.Z. Dang, C.D. Wang, E.T. Yu, K.S. Bouyros, J.M. Redwing, *Appl. Phys. Lett.* **72**, (1998) 21.
- [44] J.Z. Li, J.Y. Lin, H.X. Jiang, J.F. Geisz, S.R. Kurtz, *Appl. Phys. Lett.* **75**, (1999) 13.
- [45] R.A. Smith, "Semiconductors", Cambridge University Press (UK 1959).
- [46] R.Swanepoel, *J. Phys. E, Sci. Instrum.* **16** (1983) 1214.
- [47] R.Swanepoel, *J. Phys. E, Sci. Instrum.* **17** (1984) 896.
- [48] H. Fujiwara, "Spectroscopic Ellipsometry-Principles and Applications", John Wiley (NY 2007).
- [49] C. Cifuentes, M. Botao, E. Romero, C. Caldero, G. Gordillo, *Braz. J. Phys.* **36**. (2006) 1046.
- [50] H. Saraf, M. Merdan, O.F. Yuskel, *Turk. J. Phys.* **26**, (2002) 341.
- [51] J.Tauc, *Mat Res Bull* **5**, (1970) 721.
- [52] X. Gou, J. Chen, P. Shen, *Mater. Chem. Phys.* **93** (2005) 557.
- [53] J.I.Pankove, "Optical processes in semiconductors" (NY: PHI, 1971).
- [54] J.Xu, Y.Yang, Z.Xie, *Chalcogenide Lett.* **11**, (2014) 485.
- [55] L.L.Cheng, M.H.Liu, M.X.Wang, S.C.Wang, G.D.Wang, Q.Y.Zhou, Z.Q.Chen, *J Alloy Compd* **545** (2012) 122.
- [56] P.Pramanik, P.K.Basu and S.Biswas, *Thin Solid Films* **150**, (1987) 269.